JOURNAL OF GEOPHYSICAL RESEARCH, VOL. 105, NO. E3, PAGES 6961-6969, MARCH 25, 2000

Surface properties of Mars' polar layered deposits and polar landing sites

Ashwin R. Vasavada,[1] Jean-Pierre Williams,[1] David A. Paige,[1]
Ken E. Herkenhoff,[2] Nathan T. Bridges,[3] Ronald Greeley,[4]
Bruce C. Murray,[5] Deborah S. Bass,[6] and Karen S. McBride[1]

Abstract. On December 3, 1999, the Mars Polar Lander and Mars Microprobes will land on the planet's south polar layered deposits near (76°S, 195°W) and conduct the first in situ studies of the planet's polar regions. The scientific goals of these missions address several poorly understood and globally significant issues, such as polar meteorology, the composition and volatile content of the layered deposits, the erosional state and mass balance of their surface, their possible relationship to climate cycles, and the nature of bright and dark aeolian material. Derived thermal inertias of the southern layered deposits are very low (50-100 J m^{-2} $s^{-½}$ K^{-1}), suggesting that the surface down to a depth of a few centimeters is generally fine grained or porous and free of an appreciable amount of rock or ice. The landing site region is smoother than typical cratered terrain on ~1 km $pixel^{-1}$ Viking Orbiter images but contains low-relief texture on ~5 to 100 m $pixel^{-1}$ Mariner 9 and Mars Global Surveyor images. The surface of the southern deposits is older than that of the northern deposits and appears to be modified by aeolian erosion or ablation of ground ice.

1. Introduction

The landed component of the Mars Surveyor 1998 missions, the Mars Polar Lander (MPL), and the two New Millennium Microprobes will reach the south polar region of Mars on December 3, 1999. The lander's cameras, meteorology instruments, and thermal/evolved gas analyzer will study the subsurface, surface, and atmosphere near its landing site. The Microprobes [*Smrekar et al.*, 1999] carry thermal and evolved-water experiments. Both investigations are focused on understanding the distribution of volatiles (water and CO_2) and the present and past climate.

The MPL and Microprobes will land on the south polar layered deposits, which partially cover the region poleward of 70°S latitude [*Tanaka and Scott*, 1987]. Like on Earth, the polar regions of Mars are strongly influenced by seasonal and climatic cycles, making them ideal sites for landed experiments. The MPL will make in situ observations of temperature, atmospheric pressure, and wind, as well as the daily and seasonal exchange of volatiles such as CO_2 and water between the subsurface, surface, and atmosphere. Ground ice may be found within the 0.5-m vertical reach of its robotic arm [e.g., *Leighton and Murray*, 1966]. The stratigraphy within the layered deposits is thought to be related to variations in Mars' orbital and axial elements, which in turn modulate the loading, transport, and deposition of atmospheric water and dust. The MPL's robotic arm camera can image layering within excavated trenches, while the panoramic camera will search for layering exposed on nearby surface slopes. Seven calorimeters and an evolved gas analyzer will determine the amounts of CO_2 and water (including hydrated minerals) in accessible surface materials. The Microprobes will estimate the water content and thermal properties of the near-surface layer at a depth of ~0.3-1 m.

The range of target landing sites for MPL is limited by atmospheric entry constraints to latitudes between 74° and 76°S. These latitudes intersect a contiguous, dissected plateau of layered deposits between 170°W and 230°W longitude known as Ultimi Lobe [*Tanaka and Scott*, 1987; *Schenk and Moore*, this issue]. The maps presented by *Schenk and Moore* [this issue] provide an overview of the geology and topography of the region. Figure 1 of the present work is a Viking Orbiter mosaic showing the area accessible to MPL. The deposits appear thickest (~2 km) toward the western part of this region. As shown in Figure 2a, Ultimi Lobe forms a broad plateau west of 205°W with elevations between 4200 and 4500 m above the 6.1-mbar reference surface. Between 170° and 205°W, elevations decrease to ~2600 m along an approximately northeast gradient [M. Zuber and D. Smith, personal communication, 1999; *Smith and Zuber*, 1998].

On August 25, 1999, NASA selected MPL's primary landing site, 76°S planetocentric latitude and 195°W longitude. The Microprobes will impact ~50 km to the northwest. The simulated dispersion of actual landing sites around the target point is bounded by an ellipse with dimensions of ~240 and ~20 km, respectively (Figure 1). The flight path is poleward along the major axis of the ellipse, which points 13.5° east of south. The site was chosen by NASA on the basis of a review by the Mars Surveyor Operations Project at the Jet Propulsion Laboratory, inputs from engineering teams, and a

[1]Department of Earth and Space Sciences, University of California, Los Angeles.
[2]United States Geological Survey, Flagstaff, Arizona.
[3]Jet Propulsion Laboratory, Pasadena, California.
[4]Department of Geology, Arizona State University, Tempe.
[5]Division of Geological and Planetary Sciences, California Institute of Technology, Pasadena.
[6]Southwest Research Institute, San Antonio, Texas.

Paper number 1999JE001108.
0148-0227/00/1999JE001108$09.00

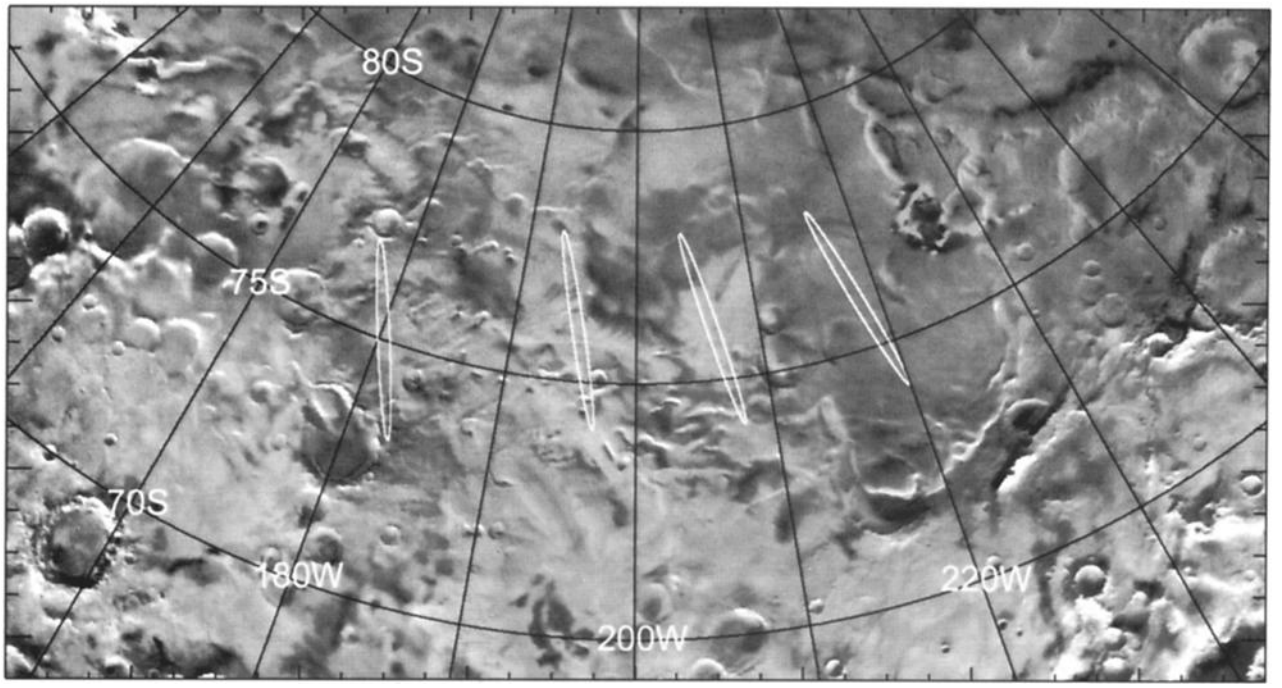

Figure 1. Viking Orbiter digital image mosaic of the landing site region in south polar stereographic projection with a central longitude of 200°W. The mosaic has been rotated westward around the south pole by 0.63° to align surface features with more accurately positioned Mars Orbiter Laser Altimeter (MOLA) elevations. At the finest scales visible in this mosaic, the Ultimi Lobe of layered deposits (near 75°S, 220°W) appears smooth relative to the surrounding cratered terrain. The distribution of dark material appears to be controlled topographically by scarps and depressions within the deposits and by impact craters on the surrounding terrain. The ellipses (see text) mark the locations of four candidate landing sites centered at (75°S, 180°W), (76°S, 195°W), (76°S, 206°W), and (76°S, 218°W). The second site was selected by NASA as the primary landing site of the Mars Polar Lander.

series of scientific workshops and studies (including this work). Engineering constraints required that the landing ellipse be placed upon a relatively smooth, flat surface with sparse coverage of rock, seasonal frost, or ice. Science considerations favored a site where material typical of the polar layered deposits in albedo, thermal inertia, morphology, and elevation might be accessible to the robotic arm and the panoramic camera. Mariner 9 and Viking Orbiter data allowed seasonal frost, kilometer-scale topographic obstacles, and atypical dark surfaces to be identified. Recent data from the Mars Orbiter Camera (MOC) and Mars Orbiter Laser Altimeter (MOLA) aboard the Mars Global Surveyor (MGS) spacecraft greatly aided the selection effort by providing measures of surface roughness (from both photometric and topographic variation), elevation, and regional slope. Because of the proprietary nature of these data, they are only summarized in the present work.

In anticipation of the landed missions, we review the current understanding of the surface properties of the south polar layered deposits, including new thermal inertia results and MGS data. The success of the missions' experiments depends greatly on the safety and scientific utility of the immediate landing site area. Currently, however, surface properties and processes can be inferred only from remotely sensed or theoretical results. We discuss the derived geologic, topographic, optical, and thermal properties of the landing site region and neighboring terrain. We begin by reviewing the spacecraft exploration of the region. We then discuss key issues in greater detail and summarize the properties of the landing site region.

2. Spacecraft Exploration of the South Polar Layered Deposits

2.1. Mariner 4, 6, 7, and 9

The first images to resolve Mars' surface features were acquired by Mariner 4 in 1965 and revealed Moon-like cratered highlands typical of the midlatitude southern hemisphere. In 1969, Mariner 6 and 7 returned images of the south polar region between 235°W and 40°W longitude during southern winter. From these images, *Sharp et al.* [1971] noted the influence of topography on the thickness and retreat of seasonal frost and the widespread evidence for erosion of the underlying surface.

In 1971, Mariner 9 became the first spacecraft to orbit Mars. The geometry of its orbit resulted in excellent observations of the south polar region. In addition, the temporal and spatial coverage of the images permitted the first geologic overview of the region. *Murray et al.* [1972] identified three geologic units, excluding the residual ice cap: (1) heavily cratered terrain, the ancient basement of the entire southern hemisphere, (2) pitted plains, the moderately cratered terrain containing the erosional features first observed in Mariner 7

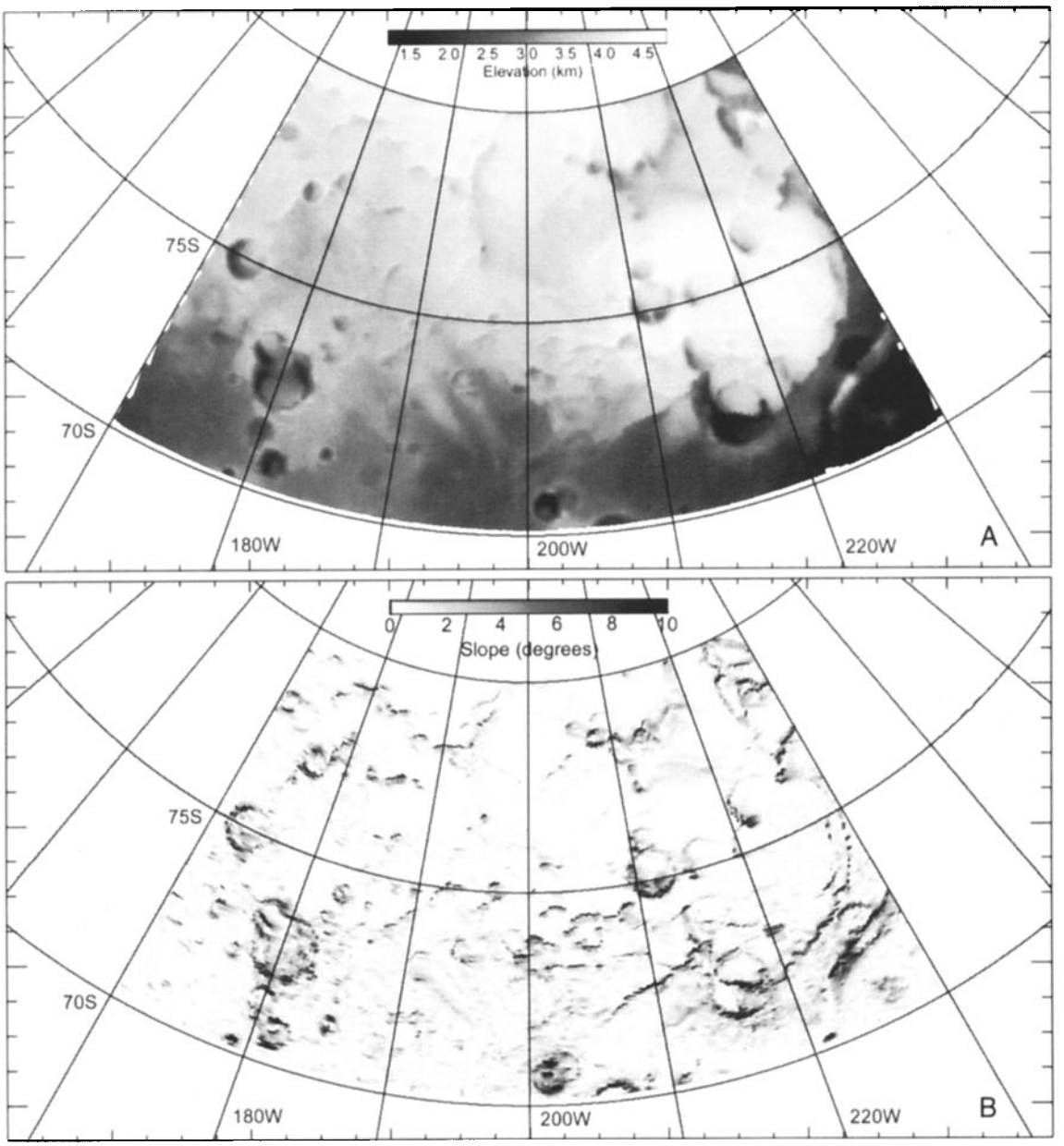

Figure 2. Polar stereographic maps of elevation and regional slope. Figure 2a displays elevation measurements acquired by the Mars Orbiter Laser Altimeter (MOLA) and referenced to the 6.1-mbar pressure surface [*Smith and Zuber*, 1998]. Measurements were linearly interpolated along lines of constant latitude between adjacent MOLA ground tracks. Figure 2b shows the along-track slope computed from pairs of adjacent MOLA measurements and interpolated as described above. Black regions have slopes which exceed MPL's safety margin of 10°. The spatial resolution of measurements in the north-south direction is near its sampling interval of 300 m. The east-west resolution is determined by the spacing between roughly north-south ground tracks. These maps were created early in MOLA's mapping period when ground tracks were spaced ~10 km apart.

images, and (3) laminated terrain (now called layered deposits), a sparsely cratered unit consisting of near horizontal strata of different textures and albedos cropping out in slopes with a range of inclinations. On the basis of impact crater counts and geometric relationships, they speculated that the residual ice cap is at the top of the stratigraphic column, followed by the layered deposits, pitted plains, and heavily cratered terrain. The units increase in age down the column and, except perhaps for the residual ice, are separated by unconformable contacts. The widespread exposures of lower units and the presence of erosional features led to the conclusion that exogenic processes, such as wind, have extensively sculpted and exhumed parts of the region.

It was immediately theorized that the layers contain a record of deposition over climatic timescales. It was further speculated that the deposition rates of airborne dust and condensing CO_2 or water ice may vary with cyclical changes in Mars' climate owing to variations in Mars' orbital and axial

parameters [*Murray et al.*, 1972; *Cutts*, 1973b]. Theoretical calculations found 10^5- and 10^6-year cycles in the magnitude and distribution of Mars' insolation that could shift CO_2 between polar cap and atmospheric reservoirs [*Ward et al.*, 1974] and influence the amount and transport of water and dust. A later analysis of high-resolution (~80 m pixel^{-1}) Mariner 9 images showed that the layered appearance in the south is due to both the retention of frost on terraces and the presence of slopes of about 10°-20° [*Herkenhoff and Murray*, 1990b]. These results imply that the physical properties of each layer are distinct and perhaps are functions of each layer's dust/ice ratio.

2.2. Overview of Viking Orbiter Results

The Viking Orbiter observations added many details to the existing framework. Layers as thin as 14 m and 100 m were resolved in the north and south, respectively [*Blasius et al.*, 1982; *Herkenhoff and Murray*, 1990b]. Sequences of layers could be followed for tens of kilometers within some outcrops, suggesting that the layers were deposited (from atmospheric condensation and/or suspension) uniformly and contemporaneously over wide areas. The few observed unconformities are possible evidence for intervening episodes of erosion [*Cutts et al.*, 1976]. They may also indicate resculpting of the deposits by local sublimation and deposition [*Howard et al.*, 1982]. The total thickness of the deposits relative to the surrounding terrain is ~3 km beneath the residual ice caps in both hemispheres. Their average thickness is between 1 and 1.5 km at lower latitudes in the south [*Schenk and Moore*, this issue].

Several theoretical models of layer formation and evolution were developed to interpret the Viking images. Within the boundary of the residual ice cap in the northern hemisphere, layers are exposed in curvilinear troughs which dissect flat or gently undulating ice-covered plains [e.g., *Cutts et al.*, 1979]. End-member scenarios interpret these troughs (1) as the result of mechanical erosion into a single, continuous stack of layers (e.g., wind-carved channels) [*Cutts*, 1973b], (2) as the by-product of preferential accumulation of sediment upon previously ice-covered surfaces [*Cutts et al.*, 1979], or (3) as continually evolving through insolation-driven sublimation and redeposition [*Howard*, 1978; *Howard et al.*, 1982]. The model of *Squyres* [1979] incorporates elements of all three scenarios. The various ideas are reviewed in more detail by *Carr* [1982] and *Thomas et al.* [1992].

The southern layered deposits contrast with those in the north in several fundamental ways. In the south, outcrops of layers are observed not only within the margin of the residual ice cap, but also within expansive lobes of layered material that extend to lower latitudes. These lobes appear to be smooth or gently undulating (at the scale of 0.1 to 1 km pixel^{-1} images), but unlike much of the northern deposits, they are not covered by residual ice. Layers in the south crop out in equator-facing escarpments or highly asymmetric troughs, in contrast with the more symmetric troughs in the north [*Schenk and Moore*, this issue; *Zuber et al.*, 1998].

The Mars Atmospheric Water Detector measured a summertime increase in water vapor over the north polar region but not the south [*Davies*, 1981]. This result is consistent with the thermally derived surface properties of the layered deposits (discussed below), namely, that the northern deposits contain water ice exposed at the surface, while the southern deposits are capped by a few centimeters of low thermal inertia material which may thermally and/or diffusively protect any ice in the deposits from sublimation [*Paige et al.*, 1994; *Paige and Keegan*, 1994; *Hofstader and Murray*, 1990].

2.3. Mars Global Surveyor

Among many anticipated contributions from MGS, the combination of high-resolution MOC images and corresponding MOLA topographic profiles will revolutionize our understanding of the stratigraphy of the deposits. Images and topographic data relevant to the landing site selection are discussed below. Further discussion of these recent results is beyond the scope of this paper.

3. Results Relevant to the Mars Polar Lander and Microprobes

Here we describe in greater detail several topics that are of prime importance for the interpretation of scientific results from the MPL and Microprobes. We review the current understanding of each topic here and integrate them in the following section.

3.1. Surface Age of the Layered Deposits

The southern layered deposits lie unconformably upon units classified as Noachian to Middle Hesperian (4.5 to 3.3 Ga) [*Tanaka and Scott*, 1987]. On the basis of the presence of 15 impact craters between 0.5 and 23 km in diameter, *Plaut et al.* [1988] estimated a surface age of at least 120 Ma and an obliteration (sedimentation or erosion) rate no greater than 8 ± 2 m Ma^{-1}. A recent reanalysis incorporating new estimates of impact fluxes yields a minimum surface age estimate in the south of 7.3 ± 3.6 Ma, or a resurfacing rate of 120 +36/-46 m Ma^{-1} (K. E. Herkenhoff and J. J. Plaut, unpublished data, 1999). In contrast, the northern layered deposits lie upon units mapped as Early to Middle Amazonian (the most recent epoch). No impact craters larger than 300 m have been found in the north, implying either a maximum age of ~0.1 Ma or an obliteration rate of at least 4000 ± 1300 m Ma^{-1} [*Cutts et al.*, 1976; *Herkenhoff et al.*, 1997]. Therefore the current estimates of surface ages and resurfacing rates differ between poles by at least two orders of magnitude and a factor of ~33, respectively. These differences caution against either assuming that the poles have similar geologic histories or extrapolating results obtained at one pole to the other.

3.2. Surface Thermal Properties

Paige et al. [1994] and *Paige and Keegan* [1994] used Viking Infrared Thermal Mapper (IRTM) 20-μm brightness temperatures to derive thermal inertia and thermally derived albedo poleward of 60° latitude in both hemispheres. Thermal inertia measures the thermal response of a surface layer to variations in incident energy and is given here in SI units (J m^{-2} s$^{-½}$ K^{-1}). The results are representative of the surface down to the diurnal thermal skin depth (a few centimeters).

Paige and Keegan [1994] found that the average thermal inertia of the polar layered deposits in the south is 168, significantly lower than their value of 565 in the north. Their interpretation was that the southern deposits are devolatilized or mantled by low thermal inertia material to a depth of at least a few centimeters, while the northern deposits probably contain

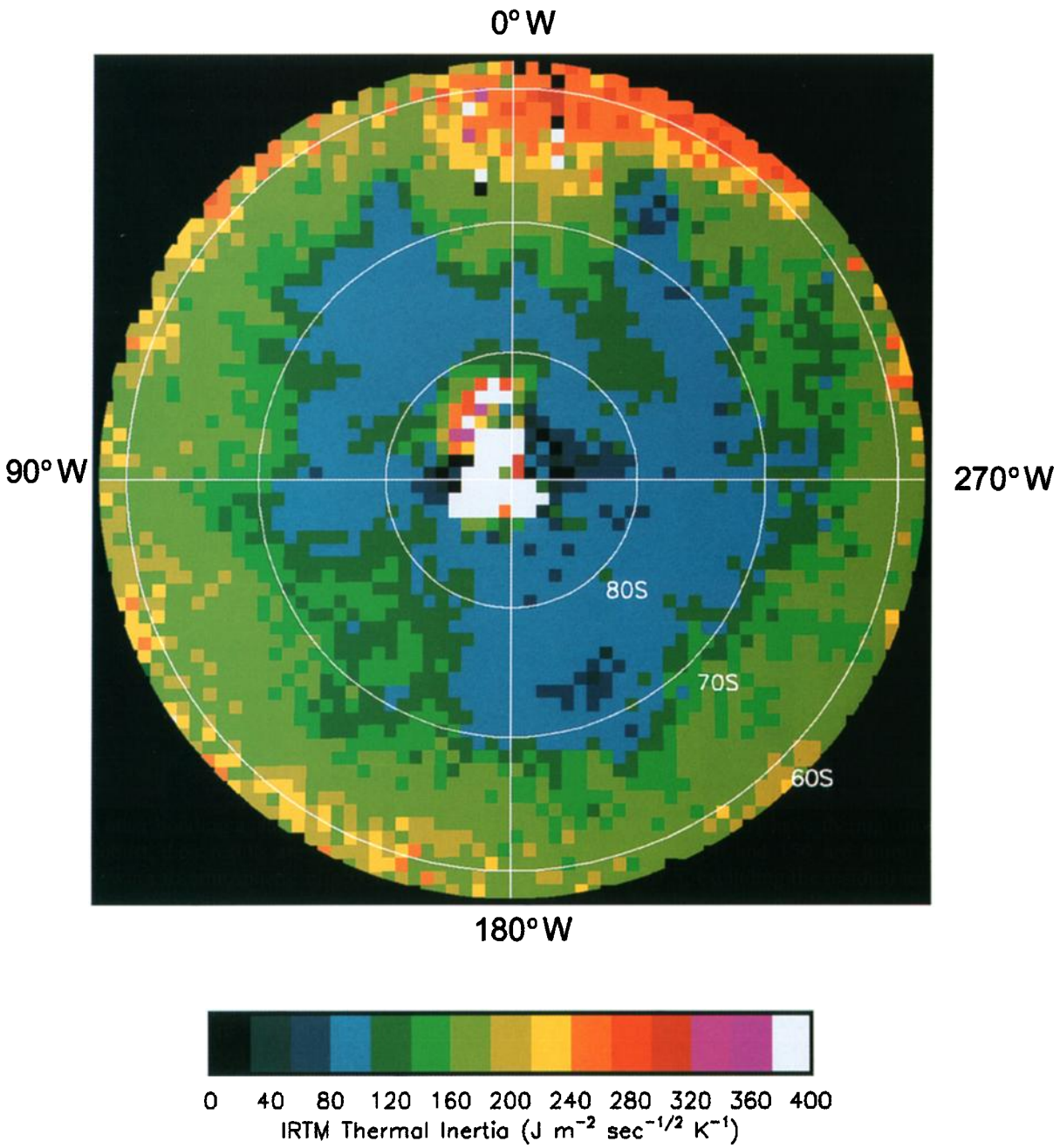

Plate 1. Derived thermal inertia poleward of 60°S latitude. This polar stereographic map was created by fitting the results of a 1-D surface-atmosphere thermal model to Viking IRTM 20-μm measurements. Inertias with values > 400 J m^{-2} s$^{-½}$ K^{-1} are plotted in white. The measurements were made during late southern summer (L_s=321°-338°).

water ice or some other bonding agent near the surface. While their analysis is robust, their results are systematically offset to higher values owing to atmospheric effects not explicitly accounted for in their derivation.

We have derived new thermal inertias for both polar regions using a coupled surface-atmosphere model [*Paige et al.*, 1994; *Herkenhoff and Vasavada*, 1999]. A description of our methods is included in the appendix. The north polar layered deposits have thermal inertias of ~450-600. Geologic units in the northern hemisphere mapped as aeolian deposits or degraded lava flows have inertias of ~50-150. The south polar layered deposits (Plate 1) have thermal inertias of ~50-100. Inertias between ~50 and 150 are found over all surfaces poleward of 70°S, excluding the residual ice cap. The boundary of this low-inertia region does not follow geologic contacts mapped from orbiter images. This may indicate that several geologic units share a common near-surface property (e.g., physical or compositional). The boundary is not a simple function of latitude either, which would have suggested a problem with the model. While only relevant for a surface composed of unconsolidated, well-sorted particles, an apparent particle size of ~10 μm can be inferred from laboratory

thermal conductivity measurements of well-sorted glass beads at relevant atmospheric pressures [*Presley and Christensen*, 1997]. More generally, the low inertias imply that the near surface over wide areas is fine grained or porous and free of an appreciable amount of rock or ice.

3.3. Surface Optical Properties

Herkenhoff and Murray [1990a] classified surface materials in the south polar region on the basis of color and albedo. Bright red dust appears to be the major nonvolatile component of the layered deposits, possibly along with a minor dark component. They found little detectable color change between the layered deposits near the pole and the surrounding terrain, perhaps indicating that a continuous mantle overlies both units. The mantle appears to have been removed from some areas, exposing the darker, less red layered deposits. The Lambert albedo map of *Paige and Keegan* [1994] also shows that the southern layered deposits lack a distinct albedo boundary.

3.4. Sublimation-Derived Mantle

Water ice is currently not stable at the surface of the layered deposits in the south polar region [*Toon et al.*, 1980; *Paige*, 1992]. Under present conditions a water ice layer equivalent to the entire thickness of the layered deposits would sublimate in about 10^4 years [*Hofstader and Murray*, 1990]. A natural consequence of sublimation is the concentration of the nonvolatile components at the surface of the deposits. A surface lag deposit could reduce further sublimation, either by limiting diffusion or by insulating the ice from extreme surface temperatures [*Toon et al.*, 1980; *Hofstader and Murray*, 1990]. It may be composed of typical atmospheric dust or more exotic material such as that described below. Some cementing agent or bonding process is probably necessary to support observed scarp slopes of up to 20° and to prevent removal of the material by winds [*Herkenhoff and Murray*, 1990b].

3.5. Dark Aeolian Material

Dark, dune-forming material is distributed over both polar regions. In the north, dark material is closely associated with the locations of steep, arcuate scarps in the layered deposits [*Thomas and Weitz*, 1989]. The material appears to be eroding from the layered deposits and collecting in the north circumpolar sand sea and smaller dune fields [*Thomas*, 1982; *Thomas and Weitz*, 1989]. In the south, material with similar color and albedo is associated with depressions and equator-facing scarps in the layered deposits and with dune fields within nearby impact craters [*Herkenhoff and Murray*, 1990a; *Thomas and Gierasch*, 1995]. However, dark material in the south has not been tied genetically to the erosion of the deposits. Differences in surface atmospheric pressure or circulation, topography, or surface age between poles may account for the lack of a circumpolar sand sea in the south [*Thomas and Gierasch*, 1995]. Several dark albedo features on the surface of the southern deposits have changed in appearance between successive Viking observations, indicating very thin mantling deposits and the mobility of either the dark or bright aeolian material [*Herkenhoff et al.*, 1999].

The dark material within the northern circumpolar sand sea has a very low derived thermal inertia of ~75 [*Herkenhoff and Vasavada*, 1999]. Its low inertia can be reconciled with its apparently sand-size grains if it is composed either of basaltic ash fragments or of aggregates of a minor, dark component of the layered deposits that form as a sublimation residue [*Storrs et al.*, 1988; *Herkenhoff and Murray*, 1990a; *Herkenhoff and Vasavada*, 1999]. Although not well-resolved in thermal inertia maps, the dark material in the south appears to have the very low inertia typical of the south polar region.

3.6. Surface Roughness

In Viking images of the southern layered deposits with spatial resolutions >100 m pixel^{-1} (e.g., Figure 1), the smooth surface of the broad plateau of deposits near 75°S and 200°W-230°W is interrupted only by low-relief, E-W striking ridges and the rims of partially buried impact craters. Ridge slopes are ≤10°, as indicated by images taken at low Sun angles. These ridges may be similar to those found on the northern deposits which were thought by *Cutts et al.* [1979] to be the surface expressions of previous (now buried) margins of the residual ice cap. *Schenk and Moore* [this issue] conjecture that they could also be interpreted as thrust faults within the deposits that are oriented parallel to the deposits' margins. Gently undulating topography has recently been cited as evidence for viscous flow of the northern layered deposits, as flow tends to smooth topography with spatial scales much less than the thickness of the deposits [*Zuber et al.*, 1998]. Regions where the deposits are very thin or absent have kilometer-scale roughness typical of the underlying cratered terrain.

At resolutions <100 m pixel^{-1}, the surface of the southern layered deposits displays considerable texture. *Cutts* [1973b, p. 4234] noted that the surface "is not smooth but displays a considerable amount of topographic relief at the smallest scales visible" on the first Mariner 9 images of the region. Grooves, flutes, and pits have been noted, suggesting mechanical erosion most likely from wind [*Cutts*, 1973a]. Figure 3 displays examples of small-scale surface textures near MPL's landing site area. The highest-resolution, springtime MOC images appear to reveal a surface nearly completely covered by low-relief mounds and pits with horizontal dimensions of tens to hundreds of meters.

4. Summary and Discussion

The presence of a residual water ice cap in the northern hemisphere and the younger surface age of the northern layered deposits argue that deposition and/or erosion have recently been more active there than in the south. The presence of thermally unstable, near-surface water ice in the northern layered deposits and their close association with what is perhaps sublimation-derived material (the dark, circumpolar dunes) are evidence for recent erosion in particular. The southern deposits are covered by a generally older and ice-free surface layer characterized by low thermal inertia. If ice is present within the deposits, its sublimation may be currently limited by a surface layer of aeolian material or by a sublimation lag. The grooves inscribed on the southern deposits indicate that wind erosion may be a more significant process in their recent history. Isolated patches of layered material and residual ice "outliers," the presence of erosional debris at both poles, and the exposure in places of layers along the margin of the deposits suggest that the present layered deposits may be erosional remnants of more areally extensive past deposits [*Tanaka and Scott*, 1987]. However, al-

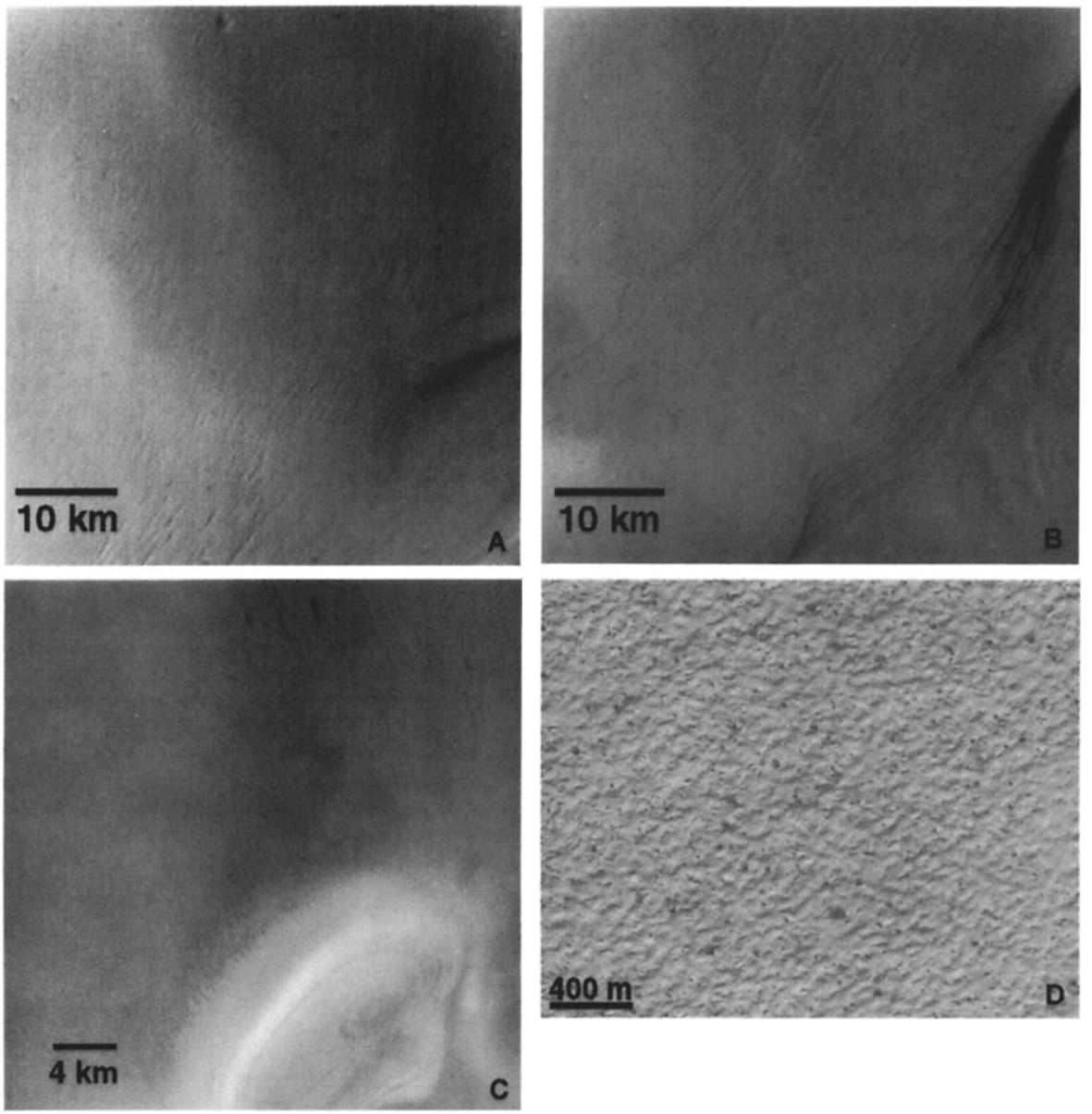

Figure 3. Surface textures of the south polar layered deposits. (a) The surface of Ultimi Lobe near (73.5°S, 223°W) during late southern summer (L_s = 346). In this Mariner 9 image (DAS 8367809; 84 m pixel^{-1}) south is toward the upper right, while the illumination is from the left. The N-S striking grooves visible on this image are widely distributed over Ultimi Lobe, although they are more apparent near its margin. The grooves have widths of a few hundred meters and lengths of several kilometers. An impact crater is located near the top center of the image. (b) The inner scarp of the western double margin of Ultimi Lobe near (75°S, 228°W) during late southern summer (L_s = 344). In this Mariner 9 image (DAS 8080243; 73 m pixel^{-1}) south is toward the upper right, while the illumination is from the left. Individual layers are easily recognized. The grooves apparent in the top center of the image appear to be formed by the erosion of a discrete layer. (c) The surface of Ultimi Lobe near (74°S, 212°W) during late southern spring (L_s = 256). In this MOC image (9503; 17 m pixel^{-1}), south is toward the top, while the illumination is from the bottom. The lower part of the image falls within a re-entrant near the margin of Ultimi Lobe. An elliptical depression at the southern end of this re-entrant has several layers exposed on its walls. In the upper part of the image the surface of the deposits contains texture at the limit of resolution as well as grooves similar to those shown in Figures 3a and 3b. (d) Highest-resolution (~5 m pixel^{-1}) view of the surface of the polar layered deposits near MPL's primary landing site of (76°S, 195°W). In this MOC image (Malin et al., Mars Polar Lander Site Surface Details, NASA's Planetary Photojournal, available at http://photojournal.jpl.nasa.gov/, 1999) south is toward the top, while the illumination is from the bottom. It was taken near southern spring equinox (L_s = 180), when seasonal CO_2 frost covered most of the surface.

ternate hypotheses, such that the deposits are present (and perhaps in steady state) within favorable local microclimates, or that they initiated and expanded in specific regions, remain viable.

Theoretical models of Mars' orbital history and its influence upon the polar climate and sedimentary processes [*Toon et al.*, 1980; *Cutts and Lewis*, 1982; *Bills*, 1990] have not been able to account for the substantial difference in surface age between hemispheres. The surface ages given above imply that the processes operative at the two poles have differed for a longer time than can be related to climate forcing from eccentricity or obliquity variations (which occur with periods of 10^5 and 10^6 years). This failure of current models currently precludes any straightforward interpretation of the record contained in the layered deposits based on astronomically forced climate change.

Much of the south polar region is of similar color, albedo, and thermal inertia. The continuity in color and albedo can be explained by the widespread presence of at least ~10 μm of bright dust [*Herkenhoff and Murray*, 1990a]. However, the low thermal inertia results are representative of a layer at least a few centimeters thick. Accordingly, the south polar region may be mantled by at least a few centimeters of typical Mars dust or perhaps by a sublimation lag deposit. The erosion (sublimation) of the layered deposits at both poles may produce the dark, low-inertia material which collects in topographic traps and is transported by saltation. The possible polar origin of this dark material and its relationship to the more ubiquitous bright material are key unknowns. For example, the darker, less red regions within the layered deposits (not within depressions or craters) may be regions where bright material has been removed, exposing the true color of the layered deposits, or may be unresolved accumulations of dark material.

The possibility that a dust mantle or sublimation lag covers the southern layered deposits raises the question of whether MPL's robotic arm will be able to access the "pristine," presumably volatile-rich layered deposits. The thickness of the surface layer is highly uncertain. If a sublimation lag, its thickness may be self-limited to the length scale of either vapor or thermal diffusion [e.g., *Hofstader and Murray*, 1990]. Meter-thick, local concentrations of aeolian bright or dark material could also inhibit the lander's access to the layered deposits. These issues are poorly addressed with currently available data, although radar results provide some insight. While the radar return from the south polar layered deposits was not distinguishable from noise, it is clearly not the "stealth" radar signature indicative of meter-thick (or deeper) deposits of low-density material [*Muhleman et al.*, 1991].

An issue of major importance to the safety of MPL is the nature of the surface at the lander's physical scale. Thermal observations indicate that the surface is generally free of rocks and boulders compared to areas such as the Viking and Pathfinder landing sites. Regional slopes appear not to pose a major hazard. Rather it is smaller features such as the grooves and texture visible at the ~10-m scale (e.g., Figure 3d) that might contain slopes that exceed the lander's safety margin of 10°. MOC images at 1.4 m pixel^{-1} acquired close to the day of landing are expected to provide the best data to assess this hazard.

Appendix: Polar Thermal Inertias With Atmospheric Corrections

Maps of polar (≥60° latitude) thermal inertias are given by *Paige et al.* [1994] and *Paige and Keegan* [1994]. Because they derived thermal inertias by comparing Viking IRTM 20-μm results to the results of a subsurface heat conduction model, their results contain systematic errors introduced by Mars' radiatively active atmosphere. The downward infrared flux from atmospheric dust inhibits the rise and fall of surface temperatures, reducing their diurnal variation for a given thermal inertia [*Haberle and Jakosky*, 1991]. In addition, the contribution to the outgoing infrared flux reduces the apparent variation detected from orbit [*Paige et al.*, 1994]. Finally, at high solar zenith angles, atmospheric dust can create an antigreenhouse effect which cools low-albedo surfaces below their radiative equilibrium temperatures [*Davies*, 1979]. Thermal inertias derived without accounting for the atmosphere will therefore exceed actual surface values. Derived albedos may exceed measured values, especially at higher latitudes.

We have used the IRTM data and methods described by *Paige et al.* [1994] and *Paige and Keegan* [1994], in conjunction with their atmospheric model, to derive new polar thermal inertias [e.g., *Herkenhoff and Vasavada*, 1999]. We chose model aerosol properties on the basis of the model's ability to reproduce the 15-μm atmospheric emissions and visible albedos measured by the IRTM. Best results were obtained with a visible opacity of 0.3 and nominal atmospheric and dust properties (see Model 6 of *Paige et al.* [1994]). We used the dust optical properties of *Clancy and Lee* [1991].

Consistent with the above discussion, our derived thermal inertias are both systematically lower and less dependent on latitude than the previous results. Albedo is derived simultaneously with inertia and provides a means of assessing the model's accuracy and self-consistency. In both hemispheres, derived albedos differ from measured albedos by <0.1. However, no combination of model dust parameters completely removed the latitudinal gradient in derived albedo (which is not observed in the measured albedos). This could be due to an anomalous, slow seasonal warming of high latitudes not accurately reproduced by the model. The thermal inertia results should not be significantly affected by such an error.

Acknowledgments. This work was part of the Mars Polar Lander site selection effort. A.V. was supported by NASA grant NAGW 5-4367. We gratefully acknowledge the Mars Orbiter Laser Altimeter and the Mars Orbiter Camera teams, especially David Smith, Maria Zuber, and Michael Malin for sharing their results and acquiring excellent data in support of the landing site selection. Gary Hansen and Alan Howard provided valuable reviews of the manuscript.

References

Bills, B. G., The rigid body obliquity of Mars, *J. Geophys. Res.*, *95*, 14,137-14,153, 1990.

Blasius, K. R., J. A. Cutts, and A. D. Howard, Topography and stratigraphy of Martian polar layered deposits, *Icarus*, *50*, 140-160, 1982.

Carr, M. H., Periodic climate change on Mars: Review of evidence and effects on distribution of volatiles, *Icarus*, *50*, 129-139, 1982.

Clancy, R. T., and S. W. Lee, A new look at dust and clouds in the Mars atmosphere: Analysis of emission-phase-function sequences

from global Viking IRTM observations, *Icarus*, *93*, 135-158, 1991.

Cutts, J. A., Wind erosion in the Martian polar regions, *J. Geophys. Res.*, *78*, 4211-4221, 1973a.

Cutts, J. A., Nature and origin of layered deposits of the Martian polar regions, *J. Geophys. Res.*, *78*, 4231-4249, 1973b.

Cutts, J. A., and B. H. Lewis, Models of climate cycles recorded in Martian polar layered deposits, *Icarus*, *50*, 216-244, 1982.

Cutts, J. A., K. R. Blasius, G. A. Briggs, M. H. Carr, R. Greeley, and H. Masursky, North polar region of Mars: Imaging results from Viking 2, *Science*, *194*, 1329-1337, 1976.

Cutts, J. A., K. R. Blasius, and W. J. Roberts, Evolution of Martian polar landscapes: Interplay of long-term variations in perennial ice cover and dust storm intensity, *J. Geophys. Res.*, *84*, 2975-2994, 1979.

Davies, D. W., Effects of dust on the heating of Mars' surface and atmosphere, *J. Geophys. Res.*, *84*, 8289-8293, 1979.

Davies, D. W., The Mars water cycle, *Icarus*, *45*, 398-414, 1981.

Haberle, R. M., and B. M. Jakosky, Atmospheric effects on the remote determination of thermal inertia on Mars, *Icarus*, *90*, 187-204, 1991.

Herkenhoff, K. E., and B. C. Murray, Color and albedo of the south polar layered deposits on Mars, *J. Geophys. Res.*, *95*, 1343-1358, 1990a.

Herkenhoff, K. E., and B. C. Murray, High-resolution topography and albedo of the south polar layered deposits on Mars, *J. Geophys. Res.*, *95*, 14,511-14,529, 1990b.

Herkenhoff, K. E., and A. R. Vasavada, Dark material in the polar layered deposits and dunes on Mars, *J. Geophys. Res.*, *104*, 16,487-16,500, 1999.

Herkenhoff, K. E., J. J. Plaut, and S. A. Nowicki, Surface age and resurfacing rate of the north polar layered terrain on Mars, *Lunar Planet. Sci. Conf.*, *XXVIII*, 551-552, 1997.

Herkenhoff, K. E., N. T. Bridges, and R. L. Kirk, Geologic studies of the Mars Surveyor 1998 landing area, *Lunar Planet. Sci.*, *XXX*, 1120, 1999.

Hofstader, M. D., and B. C. Murray, Ice sublimation and rheology: Implications for the Martian polar layered deposits, *Icarus*, *84*, 352-361, 1990.

Howard, A. D., Origin of stepped topography of the Martian poles, *Icarus*, *34*, 581-599, 1978.

Howard, A. D., J. A. Cutts, and K. R. Blasius, Stratigraphic relationships within Martian polar cap deposits, *Icarus*, *50*, 161-215, 1982.

Leighton, R. B., and B. C. Murray, Behavior of carbon dioxide and other volatiles on Mars, *Science*, *153*, 136-144, 1966.

Muhleman, D. O., B. J. Butler, A. W. Grossman, and M. A. Slade, Radar images of Mars, *Science*, *253*, 1508-1513, 1991.

Murray, B. C., L. A. Soderblom, J. A. Cutts, R. P. Sharp, D. J. Milton, and R. B. Leighton, Geological framework of the south polar region of Mars, *Icarus*, *17*, 328-345, 1972.

Paige, D. A., The thermal stability of near-surface ground ice on Mars, *Nature*, *356*, 43-45, 1992.

Paige, D. A., and K. D. Keegan, Thermal and albedo mapping of the polar regions of Mars using Viking thermal mapper observations, 2, South polar region, *J. Geophys. Res.*, *99*, 25,993-26,013, 1994.

Paige, D. A., J. E. Bachman, and K. D. Keegan, Thermal and albedo mapping of the polar regions of Mars using Viking thermal mapper observations, 1, North polar region, *J. Geophys. Res.*, *99*, 25,959-25,991, 1994.

Plaut, J. J., R. Kahn, E. A. Guinness, and R. E. Arvidson, Accumulation of sedimentary debris in the south polar region of Mars and implications for climate history, *Icarus*, *75*, 357-377, 1988.

Presley, M. A., and P. R. Christensen, Thermal conductivity measurements of particulate materials, 2, Results, *J. Geophys. Res.*, *102*, 6551-6566, 1997.

Schenk, P. M., and J. M. Moore, Stereo topography of the south polar region of Mars: Volatile inventory and Mars Polar Lander landing site, *J. Geophys. Res.*, this issue.

Sharp, R. P., B. C. Murray, R. B. Leighton, L. A. Soderblom, and J. A. Cutts, The surface of Mars, 4, South polar cap, *J. Geophys. Res.*, *76*, 357-368, 1971.

Smith, D. E., and M. T. Zuber, The relationship between MOLA northern hemisphere topography and the 6.1-mbar atmospheric pressure surface of Mars, *Geophys. Res. Lett.*, *25*, 4397-4400, 1998.

Smrekar, S., et al., Deep Space 2: The Mars Microprobe Mission, *J. Geophys. Res.*, *104*, 27,013-27,030, 1999.

Squyres, S. W., The evolution of dust deposits in the Martian north polar region, *Icarus*, *40*, 244-261, 1979.

Storrs, A. D., F. P. Fanale, R. S. Saunders, and J. B. Stephens, The formation of filamentary sublimation residues (FSR) from mineral grains, *Icarus*, *76*, 493-512, 1988.

Tanaka, K. L., and D. H. Scott, Geologic map of the polar regions of Mars, *U.S. Geol. Surv. Misc. Invest. Map*, *I-1802-C*, 1987.

Thomas, P. C., Present wind activity on Mars: Relation to large latitudinally zoned sediment deposits, *J. Geophys. Res.*, *87*, 9999-10,008, 1982.

Thomas, P. C., and P. J. Gierasch, Polar margin dunes and winds on Mars, *J. Geophys. Res.*, *100*, 5397-5406, 1995.

Thomas, P. C., and C. Weitz, Dune sand materials and polar layered deposits on Mars, *Icarus*, *81*, 185-215, 1989.

Thomas, P., S. Squyres, K. Herkenhoff, A. Howard, and B. Murray, Polar deposits of Mars, in *Mars*, edited by H. H. Kieffer, et al., pp. 767-795, Univ. of Ariz. Press, Tucson, 1992.

Toon, O. B., J. B. Pollack, W. Ward, J. A. Burns, and K. Bilski, The astronomical theory of climate change on Mars, *Icarus*, *44*, 552-607, 1980.

Ward, W. R., B. C. Murray, and M. C. Malin, Climatic variations on Mars, 2, Evolution of carbon dioxide atmosphere and polar caps. *J. Geophys. Res.*, *79*, 3387-3395, 1974.

Zuber, M. T., et al., Observations of the north polar region of Mars from the Mars Orbiter Laser Altimeter, *Science*, *282*, 2053-2060, 1998.

D. S. Bass, Southwest Research Institute, P.O. Drawer 28510, San Antonio, TX 78228-0510.

N. T. Bridges, Jet Propulstion Laboratory, 4800 Oak Grove Drive, Pasadena, CA 91109.

R. Greeley, Department of Geology, Arizona State University, Box 871404, Tempe, AZ 85287-1404.

K. E. Herkenhoff, United States Geological Survey, 2255 North Gemini Drive, Flagstaff, AZ 86001-1698.

K. S. McBride, D. A. Paige, A. R. Vasavada, and J.-P. Williams, Department of Earth and Space Sciences, University of California, Los Angeles, CA 90095-1567. (ash@mvacs.ess.ucla.edu)

B. C. Murray, Mail Stop 150-21, Geological and Planetary Sciences, California Institute of Technology, Pasadena, CA 91125.

(Received June 8, 1999; revised October 11, 1999;
accepted October 12, 1999.)